# A new approach for characterizing atmospheric aerosols from spectral values of their optical depth. A simulated case study.

# Una nueva aproximación para caracterizar los aerosoles atmosféricos a partir de los valores espectrales de su espesor óptico. Un caso de estudio.

**J. L. Gómez-Amo, J. A. Martínez-Lozano, M. P. Utrillas, V. Estellés y R. Pedrós**

Grupo de Radiación Solar, Universitat de Valencia, 46100 Burjassot (Valencia), Spain

**ABSTRACT:**

We are developing a new method to determine the spectral contribution to the aerosol optical depth due to each aerosol type. An aerosol type depends directly on the procedence of the particles (marine, continental, artic, etc) and it is formed by some different pure components (mineral, soot, soluble and insoluble particles, sulphate, etc). In order to separate these contributions it is necessary to have the spectral aerosol optical thickness and aerosol size distribution. We use this distribution function to identify the different components of aerosols allowing us to reconstruct the aerosol optical depth taking into account the contribution of each type of aerosol. The validation of the method will be carried out by verifying that the spectral aerosol optical depth corresponds to the sum of the optical depths obtained for each identified aerosol type.

**Keywords:** aerosol optical depth

**RESUMEN:**

Hemos desarrollado un método para determinar la contribución al espesor óptico debida a cada tipo de aerosoles. Con el fin de separar estas contribuciones es necesario disponer de la distribución espectral del espesor óptico y de su distribución de tamaños. Usamos estas funciones de distribución para identificar los diferentes tipos de aerosoles y así reconstruir el espesor óptico teniendo en cuenta las contribuciones de cada tipo. La validación del método se lleva a cabo verificando que el espesor óptico espectral obtenido se corresponde con la suma de los espesores ópticos de los aerosoles presentes de cada tipo.

**Palabras clave:** espesor óptico de aerosoles



Recibido: 20 october 2005

**REFERENCIAS Y ENLACES.**


Angstrom, A., (1929), On the atmospheric transmission of sun radiation and on the dust in the air. *Geografis. Annal*., 11, 156-166.

D'Almeida, G.A., P. Koepke, and E. P. Shettle, (1991), Atmospheric aerosols. Global climatology and radiative characteristics, 561 pp., A. Deepak Publishing, Hampton, Virginia.

Dubovik, O., and M. D. King, (2000), A flexible inversion algorithm for retrieval of aerosol optical properties from sun and sky radiance measurements, *J. Geophys. Res*., 105, 20673-20696.

Dutton, E. G., R. Patrick, S. Ryan and J. J. DeLuisi, (1994). Features and effects of aerosol optical depth observed at Mauna Loa, Hawaii: 1982-1992", *J. Geophys. Res*., 99, 8295-8306.

Estellés, V., M.P. Utrillas, J.L. Gómez-Amo, R. Pedrós, J.A. Martínez-Lozano, (2004), "Aerosol size distributions and air mass back trajectories over a Mediterranean coastal site", *Int. J. Rem. Sens*., 25, 39-50.

Hess, M., P. Koepke, and I. Schult, (1998), Optical properties of aerosol and clouds: the software package OPAC, *Bull. Am. Meteor. So*c., 79, 831-844.

Holben B.N., T.F. Eck, I. Slutsker, D. Tanré, J.P. Buis, A. Setzer, E. Vermote, J.A. Reagan, Y.J. Kaufman, T. Nakajima, F. Lavenu, I. Jankowiak, A. Smirnmov, (1998), AERONET-A Federated instrument network and data archive for aerosol characterization, *Rem. Sensing Environ*., 66, 1-16.

Holben, B.N. et al. (23 authors), (2001), An emerging ground-based aerosol climatology: Aerosol optical depth from AERONET*, J. Geophys. Res*., 106, 12067-12097.

JGR (Special issue), (1997). Passive remote sensing of the tropospheric aerosol and atmospheric corrections of the aerosol effect *J. Geophys. Res*, 102.

King M. D., D.M. Byrne, B. M. Herman and J. A. Reagan, (1978), Aerosol size distribution obtained by inversion of spectral optical depth measurements, *J. Atmos. Sci*., 35, 2154-67.

King M.D., (1982), Sensitivity of constrained linear inversions to the selection of Lagrange multiplier, *J. Atmos. Sci*., 39, 1356-69.

King, M.D., Y. J. Kaufman, D. Tanré and T. Nakajima, (1999), Remote sensing of tropospheric aerosols from space: past, present, and future, *Bull. Am. Meteor. Soc*., 80, 2229-2259.

Martínez-Lozano, J. A., M. P Utrillas, R. Pedrós, F. Tena, J. P. Díaz, F. J. Expósito, J. Lorente, X. De Cabo, V. Cachorro, R. Vergaz, V. Carreño, (2003). Intercomparison of spectroradiometers for global and direct solar irradiance in the visible range. *J. Atmos. Ocean Tech*. 20, 997-1010.

Moorthy, K. K., S. S. Babu, and S. K. Satheesh (2003), Aerosol spectral optical depths over the Bay of Bengal: Role of transport, *Geophys. Res. Lett.*, *30*(5), 1249, doi:10.1029/2002GL016520.

Nakajima, T., Tanaka M. and Yamakuchi, T., (1983): Retrieval of the optical properties of aerosols from aureole extinction data, *App. Opt*., 22, 2951-2959.

Nakajima, T., G.. Tonna, R. Rao, P. Boi, Y. Kaufman and B. Holben, (1996): Use of sky brightness measurements from remote sensing of particulate polydispersions, *App. Opt*., 35, 2675-2686.

O'Neill, N.T., T.F. Eck, B. N. Holben, A. Smirnov, O. Dubovik and A. Royer, (2001), Bimodal size distribution influences on the variation of Angstrom derivatives in spectral and optical depth space, *J. Geophys. Res*, 106, 9787-9806.

O'Neill, N.T., T.F. Eck, B. N. Holben, A. Smirnov, A. Royer and Z. Li., (2002), Optical properties of boreal forest fire smoke derived from sun photometry, *J. Geophys. Res*, 107, 1029/2001JD000877.

Osterwald, C.R., and K.A. Emery (2000), Spectroradiometric sun photometry, *J. Atmos. Oceanic Technol.*, *17*, 1171-1188.

Pedrós, R., J. A. Martínez-Lozano, M P. Utrillas, J. L. Gómez-Amo and F. Tena (2003), Column-integrated aerosol optical properties from ground-based spectroradiometer measurements at Barrax (Spain) during the

Digital Airborne Imaging Spectrometer Experiment (DAISEX) campaigns. *J. Geophys. Res*., *108*, doi:10.1029/2002JD003331.

Remer L. A. and Y. J. Kaufman, (1998), Dynamic aerosol model: Urban/industrial aerosol, *J. Geophys. Res*., 103, 13859-13871.

Penner, J.E., L. Reaitch, D. Murphy, J. Nganga, and G. Pitari, (2001), The aerosols, their direct and indirect effects, in Climate Change: The Scientific Basis, edited by J. Hougthton, Y. Ding, D.J. Griggs, M. Noguer, P.J. van der linden, X. Dai, K. Maskell and C.A. Johson, pp. 289-348, Cambridge Univ. Press, New York.

Schwartz, S.E. and M.O. Andreae, M.O., (1966), Uncertainty in climate change caused by aerosols, *Scienc*e, 272, 1121-1122.

Shifrin, K.S., (1995), Simple relationships for the Angstrom parameter of disperse systems, *App. Opt*., 34, 4480-4485.

Smirnov, A., B. N. Holben, O. Dubovik, R. Frouin, T. F. Eck and I. Slutsker (2003), Maritime component in aerosol optical model derived from the Aerosol Robotic Network data, *J. Geophys. Res*., *108*. doi:10.1029/2002JD002701.

WMO, 1994, Report on the measurements of atmospheric turbidity in BAPMoN, GAW Report No. 94.

## 1.- Introduction

For the new generation of satellites (King et al., 1999), aerosol models which link aerosol properties to variables that can be readily measured by satellite are desirable (Remer and Kaufman, 1998). Although the algorithms employed in these models generally simulate the characteristics of the aerosols it is, however, difficult to identify what kind of aerosols are present at a certain moment and in a particular place since, usually, different kinds of aerosols are found together. Accurate information on the radiative and optical properties of the atmospheric aerosols, as well as their distribution in space and time, is needed (Schwartz and Andreae, 1996; Penner et al., 2001). In addition algorithms need to be developed to relate such properties to parameters that can be easily measured from satellite (JGR, 1997).

Aerosol optical depth (AOD) is the single most comprehensive variable for remotely assessing the aerosol burden in the atmosphere from ground based instruments, which are, in turn, the simplest, most accurate and easy to maintain monitoring systems (Holben et al., 2001). The AOD is used to characterize aerosols and, for instance, to make atmospheric corrections to satellite remotely sensed data. Currently the AERONET network (Holben et al., 1998) fills the gap left when previouos measurement networks were discontinued after their results had been widely questioned (Dutton et al., 1994; WMO, 1994).

Therefore it seems reasonable to use measurements of AOD as the starting point for obtaining the characteristics of atmospheric aerosols when they are usually a mixture of different types above a measurement site. The usual procedure consists in a parameterisation of the experimental values of AOD that does not necessarily describe the nature of the aerosols. The most widely used procedure is based on the Angstrom formulation (Angstrom 1929) and relates the AOD to the wavelength using only two parameters, known as the turbidity coefficient ($\beta$) and the wavelength exponent ($\alpha$).

$$\tau_a = \beta\lambda^{-\alpha} \qquad (1)$$

Several attempts to apply the $\alpha$ coefficient in remote sensing can be found in the literature of the last twenty years. Lately there has been an increasing interest in this question due to the work of O'Neill et al. (2001, 2002) who developed a new approach, using the Shifrin (1995) formulation, based on a geometric interpretation of the variation of AOD with wavelength.

In the present work we propose an alternative approach, based on the Mie theory, using inversion methods and aerosol microphysical properties to determine the spectral contribution to the aerosol optical thickness due to each type of aerosol. The validation of this method will be carried out by verifying that the spectral aerosol optical depth corresponds to the addition of the optical depth obtained for each identified aerosol type. This approach is currently under development and a further validation using experimental values of AOD

is required. This work describes the first stage of the approach and presents some preliminary results corresponding to simulations with different aerosol models.

## 2.- Methodology

We aim to establish a method to identify the different types and proportion of aerosols present simultaneously in an atmospheric column above a certain place. The inputs will be the AOD experimental values for several wavelengths. In principle we will limit the analysis to the visible spectrum (400-670 nm) and later apply it to UV (up to 300 nm) and NIR (up to 1100 nm), covering the whole spectral range of the spectroradiometers available in our group (Martínez-Lozano et al., 2003). In a first stage the experimental measurements will correspond to the direct solar irradiance extinction. For a greater accuracy, particularly in the inversion algorithms, we will use measurements of sky radiance in the principal and almucantar planes made with a CIMEL sunphotometer (Estellés et al., 2004).

The final objective of this work is to establish a relationship between the experimental optical depths and the optical depths corresponding to the different types of aerosol present. As a first step we will investigate whether the current inversion methods allow us to reconstruct for every wavelength, $\lambda_j$, the relationship:

$$\tau(\lambda_j) = \Sigma\, \tau_i(\lambda_j) \qquad (2)$$

where $\tau_i$ is the AOD of each type of aerosol that contributes to the total AOD ($\tau$).

If we assume that both the set of values of $\tau(\lambda_j)$ and each particular set $\tau_i(\lambda_j)$ are continual functions, though not necessarily of the Angstrom type, the final objective of this paper is to establish functional relationships between the parameters defining $\tau(\lambda_j)$ and $\tau_i(\lambda_j)$. The starting point is that: a) expression (2) is satisfied for every wavelength; and b) according to the spectral characteristics of our instruments, using only the visible spectrum (400-700 nm), at least 300 relationships in the form of (2) are available.

In this paper we present the results corresponding to the first stage of the work. We have performed simulations for combinations of aerosols with known characteristics, before applying to measured data. These combinations were obtained from the software package OPAC (Optical Properties of Aerosol and Clouds) (Hess et al., 1998). The main difference between our methodology and the geometrical approximation of O'Neill et al. (2001), apart from the mathematical algorithms used, is that we aim to determine the types of aerosols whereas O'Neill et al. focus on determining the aerosols in the fine and coarse mode of the bimodal distribution without taking into account their origin. The method introduced here has an additional difficulty as it has a physical basis instead of a geometric one. It assumes that a concrete type of aerosol can contribute (with different relative weight) to both modes of the bimodal distribution. We have to point out that this is a preliminary work and we are still a long way from establishing unequivocally functional relationships for the optical depths, if they exist.

Regarding the objectives of the present work, we have applied the following methodology:

a) Determination of the aerosol size distribution.

From the spectral values of the total AOD, $\tau(\lambda_j)$, the size distribution, $n_c(r)$, for the aerosols in an atmospheric column was determined. As the number of measurements of solar irradiance extinction is much higher that the number of measurements of sky radiance we applied the King inversion algorithm (King et al., 1978; King, 1982) to obtain the size distribution. For further studies it is scheduled to use sky radiance measurements that require more complex algorithms such as those developed by Nakajima et al. (1983, 1996) and Dubovik and King (2000).

b) Identification of the aerosol components.

The identification of the different aerosol components in the atmosphere was based on the size distribution. The starting points were the parameters that fit the sum of lognormal functions that constitute the size distribution. These fitting parameters are ($r_{Mi}$, $N_i$ y $\sigma_i$) and we compared them to the aerosol databases (D´Almeida et al., 1991; Hess et al., 1998) to identify components. This method considered the modal radius but in further studies could consider some type of combination between the tabulated components to reconstruct the modes of the size distribution more accurately. In this combination the effective radius might be more useful. Once the components that reconstruct the size distribution were obtained, the refractive index for each mode could be obtained and subsequently the extinction efficiency factor for each.

c) Calculation of the optical thickness.

The optical thickness of each type of aerosol identified in the previous section was obtained by direct integration of the Mie expression:

$$\tau_\lambda(i)=\int_{r_a}^{r_b} \pi r^2\, Q_{ei}(n,r,\lambda)\, n_{ci}(r)\, dr \qquad (3)$$

This integration can be done in different ways: a) by using the whole size distribution function, so that the total optical thickness, $\tau(\lambda_j)$, is obtained; or b) by integrating each mode separately, which allows us to determine the contribution of each mode to the total optical depth $\Sigma\tau_i(\lambda_j)$. In principle the two optical depths do not necessarily coincide as the integration procedure is different. In both cases the aerosol size distribution $n_c(r)$, is already integrated in the whole atmospheric column.

d) Validation of the method

This method was validated by comparing the optical depth obtained with experimental measurements of extinction with the sum of each individual component. In addition we can perform a simultaneous validation of the inversion method used for the size.

## 3.- Results

As a first step to validate the method we used simulations in order to control all the variables of the system. These variables included the physical parameters that characterise the aerosols (size, refractive index, etc.) and the total optical depths that resulted from the combination of several aerosol components. We refer to these combinations as types of aerosols (maritime, continental, desert, arctic, etc.).

We used these simulations to determine the total AOD using the physical parameters of the aerosols as an input (direct method) as well as to reconstruct the characteristics of the different types of aerosols using the total AOD (inverse method). We present here the results obtained for two types of aerosols in the OPAC database (Hess et al., 1998): a) continental polluted aerosols, and b) desert aerosols. The size distribution has been obtained using $r_{Mi}$, $N_i$ and $\sigma_i$, where i refers to each component of these two aerosol types. In the OPAC database the values of the maximum ($r_{max}$) and minimum ($r_{min}$) radius also appear, thus avoiding hypotheses on the integration limits.

### 3.1 Direct method: determination of the spectral AOD.

a) Continental polluted aerosol.

This type of aerosols is characteristic of urban areas that have been highly polluted by human activity. According to the OPAC software (Hess et al., 1998) the aerosols are an external mixture of three components: a) water soluble (hereafter referred to as waso50 as the relative humidity selected for the simulations was 50%); b) insoluble aerosols (inso); and c) soot. The contribution and the physical characteristics of each component of the mixture at gound level appear in Table I.

Table I. Continental polluted aerosol. Physical characteristics.

| | $N_i$ ($cm^{-3}$) | $r_{Mi}$ (μm) | $\sigma_i$ | $r_{min}$ (μm) | $r_{max}$ (μm) | Number mixing ratios ($n_i$) |
|---|---|---|---|---|---|---|
| Waso | 15700 | 0.0262 | 2.24 | 0.006 | 25 | 0.685 |
| Inso | 0.6 | 0.471 | 2.51 | 0.005 | 20 | 0.298 |
| Soot | 34300 | 0.0118 | 2.00 | 0.005 | 20 | 0.044 |
| Total | 50000 | | | | | |

In order to determine the size distribution in an atmospheric column we have to previously define the aerosol vertical profile. In our case we introduced the simplifying hypothesis that the aerosols are homogeneously distributed in the boundary layer at two kilometres above ground level. It is mean that the integral along the vertical profile is a constant value of 2 units. Applying this hypothesis to the values in Table I and assuming lognormal monomodal size distributions for each component we obtained the curves given in Figure 1. In this Figure, we have also included the curve showing the sum of the three components. It can be seen that the resulting size distribution was bimodal and that the accumulation mode was more important than the coarse mode.

From the curves given in Figure 1, we obtained the AOD values by integrating equation (3). This integration was done in the two different ways mentioned in the previous section so we obtained $\tau(\lambda_j)$ and $\Sigma\tau_i(\lambda_j)$. We used the wavelengths 350, 400, 500, 550, 610 and 670 nm. The Mie extinction factor, $Q_e(n,r,\lambda)$, depends on the radius, the wavelength and the refractive index. If we calculate the optical thickness for a single component, its refractive index is known for the spectral range that we consider. This is not the case when the integration is performed for the total size distribution. In our case we derived the refractive index from the combination of the refractive indexes of each component weighted with its number mixing ratio:

$$n=\sum_i^N n_i \nu_i\,, \qquad m=\sum_i^N m_i \nu_i \qquad (4)$$

where $n_i$ and $m_i$ are the real and imaginary part of the refractive index respectively, N is the number of components and $\nu_i$ is the number mixing ratio of each component.

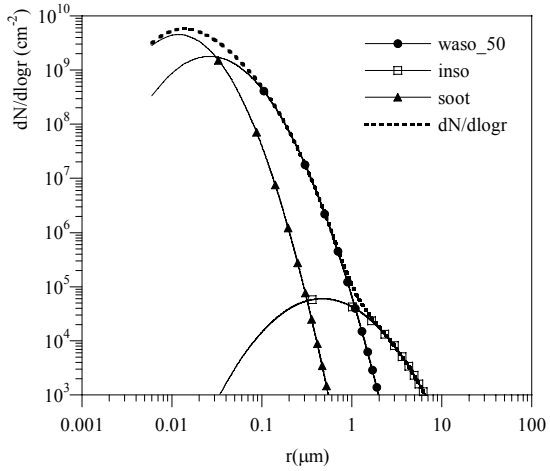


Figure 1. The size distribution for continental polluted aerosols.

The Table II shows the results of the integration using the two integration methods described above. In Figure 2 the corresponding spectral AOD curves are shown. The theoretical OPAC values were obtained using the OPAC software and also appear in Table II and Figure 2. Furthermore the deviations with respect to these theoretical values, in terms of relative MAD (Mean Absolute Deviation), are given in Table II. The most outstanding conclusion that we can draw is that the AOD obtained by adding each component, $\Sigma\tau_i$ differed by more than 30% from the results obtained when integrating directly the size distribution sum of the total sum $\tau$. If we compare both results with the OPAC AOD, $\tau_{OPAC}$, we find that the difference with $\Sigma\tau_i$ are 4-8% and practically constant over the wavelength range. However the differences between $\tau$ and $\tau_{OPAC}$ were more than 40% with a strong dependence with increasing wavelength. Table II and Figure 2 also show that the water soluble component was the main contributor to AOD, with an average value of 80%, although it was wavelength dependent. The contributions of the other two components are about 16% for soot and 4% for insoluble.

b) Desert aerosol.

This type of aerosols is used to characterise aerosols in deserts all over the world, and does not take into account local properties. These aerosols are mineral particles of different sizes distributed in three modes, nucleation (minm), accumulation (miam) and coarse (micm). A small proportion of water soluble aerosols (waso) can also appear. The physical properties of each component and their contribution to the mixture at ground level are shown in Table III (Hess et a., 1998). The size distributions for each component, obtained by integrating equation (3), appear in Figure 3. These size distributions were obtained by assuming again a boundary layer of 2 km. It can be seen that the curve for the mixture is bimodal and the difference between the heights of the modes is lower than in the previous case.

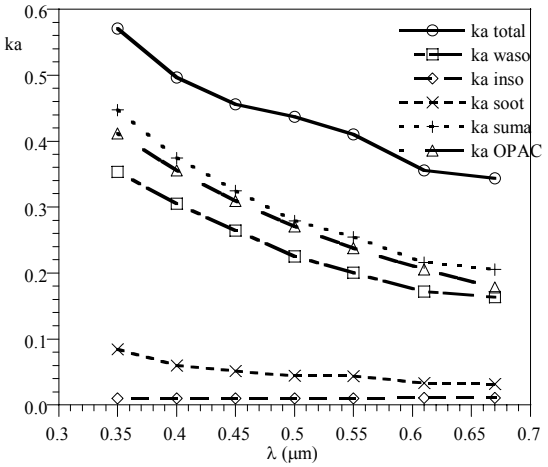


Figure 2. Continental polluted AOD.

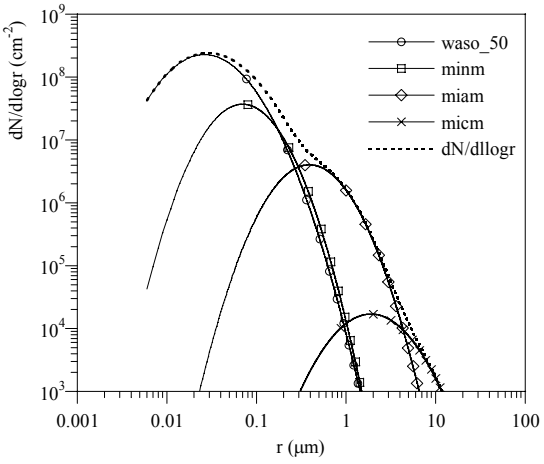


Figure 3. The size distribution for desert aerosols.

Table II. Continental polluted AOD obtained by integrating eq. (3).

| λ (nm) | τ | $\tau_{waso}$ | $\tau_{inso}$ | $\tau_{soot}$ | $\Sigma\tau_t$ | $\tau_{OPAC}$ | MAD (%) ($\Sigma\tau_i$) | MAD (%) (τ) |
|---|---|---|---|---|---|---|---|---|
| 350 | 0.5705 | 0.3531 | 0.0098 | 0.0843 | 0.4472 | 0.4115 | 8.0 | 38.6 |
| 400 | 0.4965 | 0.3048 | 0.0099 | 0.0599 | 0.3746 | 0.3556 | 5.1 | 39.6 |
| 450 | 0.4558 | 0.2640 | 0.0100 | 0.0510 | 0.3250 | 0.3930 | 4.8 | 45.1 |
| 500 | 0.4370 | 0.2250 | 0.0100 | 0.0440 | 0.2790 | 0.2704 | 3.1 | 61.6 |
| 550 | 0.4100 | 0.2006 | 0.0102 | 0.0438 | 0.2546 | 0.2376 | 6.7 | 72.5 |
| 610 | 0.3556 | 0.1721 | 0.0103 | 0.0334 | 0.2158 | 0.2058 | 4.7 | 72.8 |
| 670 | 0.3438 | 0.1634 | 0.0103 | 0.0315 | 0.2052 | 0.1780 | 0.6 | 93.1 |

Table III. Desert aerosol. Physical characteristics.

| | $N_i(cm^3)$ | $r_{Mi}$ (μm) | $\sigma_i$ | $r_{min}$ (μm) | $r_{max}$ (μm) | Number mixing ratios ($n_i$) |
|---|---|---|---|---|---|---|
| Minm | 269.5 | 0.07 | 1.95 | 0.005 | 20 | 0.018 |
| Miam | 30.5 | 0.39 | 2.00 | 0.005 | 20 | 0.033 |
| Micm | 0.142 | 1.90 | 2.15 | 0.005 | 60 | 0.747 |
| Waso | 2000 | 0.0262 | 2.24 | 0.006 | 25 | 0.202 |
| Total | 2300 | | | | | |

Following the same procedure that we used before, Table IV and Figure 4 show the retrieved spectral AOD. As Table IV shows, for this type of aerosols the values of $\Sigma\tau_i$ and τ were very similar, with differences lower than 3% for the spectral range that we used. In this case both values were higher than $\tau_{OPAC}$. The average values of the relative MAD were 11-14 % in the case of $\Sigma\tau_i$ and 13-17 % in the case of τ. The values were almost independent of wavelength, though the higher values were found for higher wavelengths. For this type of aerosol the main contribution to AOD was due to mineral particles in the accumulation mode, with 67%. The nucleation and coarse modes contributed with 15 % and 7 %, respectively, and water soluble particles with 10%.

c) Angstrom coefficient

The AOD values for the two previous cases were fitted to Angstrom-like expressions and the α value was obtained from the logarithmic linear fitting of (1). The aim of these fittings was to establish relationships between the α values for each AOD. The ideal situation would be to relate $\alpha_t$ for $\Sigma\tau_i$ with $\alpha_i$ for each $\tau_i$. From the analysis of the curves of spectral AOD a discontinuity was sometimes observed at 560 nm (Osterwald and Emery, 2000; Pedrós et al, 2003; Moorthy et al., 2003; Smirnov et al., 2003) so the fits were performed in three ranges, 350-670 nm, 350-550 nm and 550-670 nm. The results of the slope (α) and its errors associated with the linear fitting are in Table V (continental polluted aerosols) and Table VI (desert aerosols).

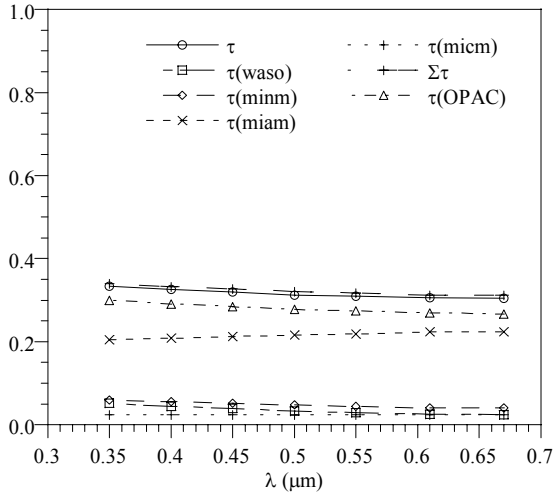


Figure 4. Desert aerosol AOD.

Table IV. Desert aerosol AOD obtained by integrating eq. (3).

| λ (nm) | τ | $\tau_{waso}$ | $\tau_{minm}$ | $\tau_{miam}$ | $\tau_{micm}$ | $\Sigma\tau_i$ | $\tau_{OPAC}$ | MAD(%) ($\Sigma\tau_i$) | MAD(%) (τ) |
|---|---|---|---|---|---|---|---|---|---|
| 350 | 0.34887 | 0.0518 | 0.0596 | 0.2050 | 0.0236 | 0.3400 | 0.2989 | 13.7 | 11.5 |
| 400 | 0.34181 | 0.0447 | 0.0560 | 0.2085 | 0.0237 | 0.3330 | 0.2911 | 14.4 | 11.8 |
| 450 | 0.33536 | 0.0387 | 0.0523 | 0.2121 | 0.0238 | 0.3269 | 0.2844 | 14.9 | 12.3 |
| 500 | 0.32950 | 0.0330 | 0.0483 | 0.2156 | 0.0239 | 0.3208 | 0.2784 | 15.2 | 12.3 |
| 550 | 0.32453 | 0.0294 | 0.0445 | 0.2191 | 0.0240 | 0.3127 | 0.2735 | 14.3 | 13.2 |
| 610 | 0.31949 | 0.0252 | 0.0401 | 0.2232 | 0.0242 | 0.3127 | 0.2683 | 16.5 | 13.5 |
| 670 | 0.31946 | 0.0240 | 0.0401 | 0.2232 | 0.0242 | 0.3114 | 0.2659 | 17.1 | 14.2 |

Table V. Continental polluted aerosols. Angstrom power exponent.

| | α (350-670 nm) | error | α (350-550 nm) | error | α (550-670 nm) | error |
|---|---|---|---|---|---|---|
| Total | 0.77 | 0.04 | 0.73 | 0.07 | 0.9 | 0.3 |
| Waso | 1.25 | 0.03 | 1.25 | 0.04 | 1.1 | 0.3 |
| Inso | -0.081 | 0.009 | -0.080 | 0.016 | -0.05 | 0.03 |
| Soot | 1.56 | 0.15 | 1.6 | 0.2 | 1.8 | 0.6 |
| Sum | 1.34 | 0.04 | 1.27 | 0.03 | 1.81 | 0.15 |
| OPAC | 1.25 | 0.03 | 1.20 | 0.03 | 1.45 | 0.04 |

Table VI. Desert aerosols. Angstrom power exponent.

| | α (350-670 nm) | error | α (350-550 nm) | error | α (550-670 nm) | error |
|---|---|---|---|---|---|---|
| Total | 0.146 | 0.009 | 0.1606 | 0.0016 | 0.08 | 0.04 |
| Waso | 1.25 | 0.03 | 1.25 | 0.04 | 1.08 | 0.26 |
| Minm | 0.67 | 0.04 | 0.63 | 0.04 | 0.5 | 0.3 |
| Miam | -0.142 | 0.008 | -0.148 | 0.004 | -0.09 | 0.05 |
| Micm | -0.037 | 0.002 | -0.038 | 0.002 | -0.029 | 0.015 |
| Sum | 0.142 | 0.008 | 0.157 | 0.004 | 0.09 | 0.03 |
| OPAC | 0.184 | 0.006 | 0.197 | 0.012 | 0.143 | 0.011 |

### 3.2 Inverse method: size distributions retrieved from spectral AOD

Using the values of optical depth sum, total and OPAC, obtained in previous cases the size distribution function has been reconstructed by inversion using the King method. With this reconstruction we can assess the validity of the King algorithm to retrieve the size distribution as well as to compare the reconstructed optical thickness with the input values.

Some of the size distributions obtained by applying the King method are shown in Figures 5 (continental polluted aerosols) and 6 (desert aerosols). We have to point out that the limitations of the King method will make the appropriate reconstruction of the modes with a modal radius greater than 1μm difficult. The different distributions were reconstructed and fitted, and the results are given in Table VII. The King method is based in an iterative inversion algorithm which look for a solution of the size distribution function. The aerosol optical depth is reconstructed using the size distribution obtained at each iteration, after that is compared with the experimental one. The procedure finish when both values of aerosol optical depth (experimental and reconstructed) are closer than a fixed quantity.

The Angstrom parameters have been recalculated from the optical thickness reconstructed using the King algorithm, in order to compare them with the results of the direct method (Tables VIII and IX). In this case fits were only performed in the range [350, 670] nm since the King algorithm uses the Angstrom expression to recalculate the optical thickness and the retrieved parameter would not change in another spectral range. The values of RMS asses how well the King algorithm can reconstruct the optical thickness. The values α King are obtained by fitting to the Angstrom expression the reconstructed optical thickness using the King method. The unlabeled α values were obtained previously by the direct method. In general, both values coincided except when the RMS discrepancies are slightly higher.

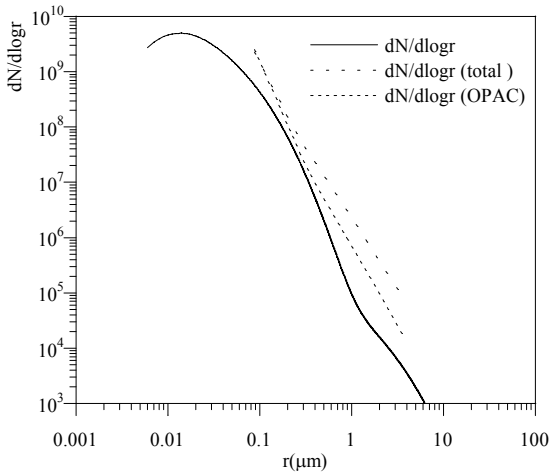


Figure 5. Aerosol size distribution obtained from King inversion algorithm. Continental polluted aerosols type.

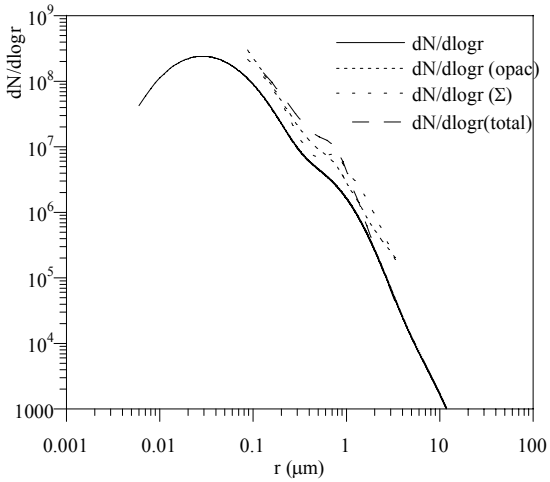


Figure 6. Aerosol size distribution obtained from King inversion algorithm. Desert aerosols type.

Table VII. Continental polluted aerosols and desert aerosol fits.

| | Continental Polluted | | | Desert | | |
|---|---|---|---|---|---|---|
| R < 0.5 | $N_i$ ($\mu m^{-3}$) | $r_{Mi}$ ($\mu m$) | $\sigma_i$ | $N_i$ ($\mu m^{-3}$) | $r_{Mi}$ ($\mu m$) | $\sigma_i$ |
| Total | $3.0\ 10^{10}$ | 0.013 | 2.2 | $1.2\ 10^{9}$ | 0.012 | 3.3 |
| Sum | $3.3\ 10^{10}$ | 0.014 | 2.2 | $1.0\ 10^{9}$ | 0.014 | 2.6 |
| Opac | $4.7\ 10^{10}$ | 0.014 | 2.1 | $2.8\ 10^{9}$ | 0.009 | 3.2 |
| R > 0.5 | $N_i$ ($\mu m^{-3}$) | $r_{Mi}$ ($\mu m$) | $\sigma_i$ | $N_i$ ($\mu m^{-3}$) | $r_{Mi}$ ($\mu m$) | $\sigma_i$ |
| Total | $1.2\ 10^{8}$ | 0.07 | 2.6 | $6.8\ 10^{6}$ | 0.52 | 3.0 |
| Sum | $2.6\ 10^{7}$ | 0.16 | 1.7 | $4.3\ 10^{6}$ | 0.63 | 3.4 |
| Opac | $3.8\ 10^{7}$ | 0.09 | 2.4 | $9.4\ 10^{6}$ | 0.30 | 3.2 |

Table VIII. Recalculated Angstrom power exponent. Continental polluted aerosols.

| | α King | $\varepsilon_\alpha$ | R | α | $\varepsilon_\alpha$ | R | RMS (%) |
|---|---|---|---|---|---|---|---|
| Total | 0.76 | 0.06 | 0.99 | 0.750 | 0.002 | 0.99 | 2.7 |
| Waso | 1.25 | 0.03 | 0.99 | 1.106 | 0.003 | 0.99 | 4.5 |
| Inso | -0.03 | 0.01 | 0.82 | -0.03 | 0.01 | 0.82 | 0.004 |
| Soot | 1.56 | 0.15 | 0.97 | 1.432 | 0.010 | 0.99 | 6.0 |
| Sum | 1.34 | 0.04 | 0.99 | 1.34 | 0.03 | 0.99 | 1.9 |
| OPAC | 1.25 | 0.03 | 0.99 | 1.25 | 0.03 | 0.99 | 0.11 |

Table IX. Recalculated Angstrom power exponent. Desert aerosols.

| | α King | $\varepsilon_\alpha$ | R | α | $\varepsilon_\alpha$ | R | RMS (%) |
|---|---|---|---|---|---|---|---|
| Total | 0.146 | 0.009 | 0.99 | 0.146 | 0.008 | 0.99 | 0.25 |
| Waso | 1.25 | 0.04 | 0.99 | 1.243 | 0.006 | 0.99 | 2.4 |
| Minm | 0.67 | 0.04 | 0.99 | 0.670 | 0.012 | 0.99 | 1.9 |
| Miam | -0.141 | 0.008 | 0.99 | -0.142 | 0.008 | 0.99 | 0.06 |
| Micm | -0.042 | 0.003 | 0.99 | -0.041 | 0.004 | 0.97 | 0.11 |
| Sum | 0.147 | 0.014 | 0.98 | 0.147 | 0.011 | 0.99 | 0.31 |
| OPAC | 0.186 | 0.006 | 0.99 | 0.186 | 0.006 | 0.99 | 0.24 |

## 4. - Conclusions

It is difficult to find clear conclusions because this work it has been only a first step in the development of this new method. In spite of that it has been possible to determine the contribution of each aerosol component to the whole mixture of aerosols. Furthermore we think that the addition of the optical thickness of each component is the best way to determine the total aerosol optical depth because no assumptions about the extinction efficiency factor are necessary. At this moment we are already working on the improvement of this technique and its validation using experimental data.